Journal of Digital Imaging (2020) 33:456–464
https://doi.org/10.1007/s10278-019-00257-5

ORIGINAL PAPER

Imaging Properties of Additive Manufactured (3D Printed) Materials for Potential Use for Phantom Models

Elizabeth Silvestro [1,2] · Khalil N. Betts [1,2] · Michael L. Francavilla [1,2,3] · Savvas Andronikou [1,2] · Raymond W. Sze [1,2,3]

Published online: 13 September 2019

Abstract

Over the last few decades, there has been growing interest in the application of additive manufacturing (AM) or 3D printing for medical research and clinical application. Imaging phantoms offer clear benefits in the way of training, planning, and quality assurance, but the model's availability per catalog tend to be suited for general testing purposes only. AM, on the contrary, offers flexibility to clinicians by enabling custom-built phantoms based on specific interests or even individual patient needs. This study aims to quantify the radiographic properties (ultrasound, magnetic resonance imaging, and computed tomography) of common additive manufacturing technologies and to discuss potential opportunities to fabricate imaging phantoms. Test phantoms were composed of samples from the three most common AM styles, namely PolyJet, fused deposition modeling (FDM), and stereolithography (SLA). Test imaging of the phantoms was performed on ultrasound, MRI, and CT and reviewed and evaluated with radiology software. The ultrasound images showed clearly defined upper and lower edges of the material but did not demonstrate distinct differences in internal echogenicity between materials. The MR scans revealed a distinct signal intensity difference between the model (17 grayscale value) and the printer support (778 grayscale value). Finally, the CT images showed a slight variation between the plastic (82 HU) and rubber (145 HU) materials. The radiographic properties of AM offer a clear opportunity to create basic two- or three-material phantoms. These would be high-accuracy and cost-effective models. Although the materials currently available are not suitable for complex multi-material applications as realistic as true human anatomy, one can easily foresee the development of new materials with broader density in the near future.

Keywords 3D printing · Additive manufacturing · Phantoms · Simulation

✉ Elizabeth Silvestro
silvestro@email.chop.edu

Khalil N. Betts
bettsk@email.chop.edu

Michael L. Francavilla
francavilm@email.chop.edu

Savvas Andronikou
andronikos@email.chop.edu

Raymond W. Sze
szer@email.chop.edu

[1] Children's Hospital Additive Manufacturing for Pediatrics (CHAMP Lab), Children's Hospital of Philadelphia, Philadelphia, PA, USA

[2] Department of Radiology, Children's Hospital of Philadelphia, Philadelphia, PA, USA

[3] Perelman School of Medicine at the University of Pennsylvania, Philadelphia, PA, USA

Abbreviations

AM	Additive manufacturing
FDM	Fused deposition modeling
SLA	Stereolithography

Introduction

Additive Manufacturing

The application of additive manufacturing (AM) in medical research and clinical use has skyrocketed within recent decades, including the development of training phantoms and simulators. New innovations have been reported in machine technology, material options, and applications. With this rapid growth in mind, this paper aims to investigate and evaluate

standard AM materials for their basic imaging properties to provide the essential baseline for these developments.

AM, also known as 3D printing, includes a variety of printing styles. The three main printing styles used for medical models are the fused deposition model (FDM), PolyJet, and stereolithography (SLA) [1]. Each printing style has benefits and drawbacks. FDM involves the process of layering melted thermoplastic using a motor-driven head; it is excellent for larger, less expensive models, but tends to be less accurate due to the relatively large nozzle size and rigging mechanisms. PolyJet, in comparison, involves the process of layering liquid photopolymers that are immediately hardened with ultraviolet (UV) light. PolyJet provides the opportunity to create a model with a large variety of distinct imaging qualities in one print with high dimensional accuracy, but this technology can be limited by the forceful support removal process that can cause damage to small features. SLA, last but not least, works by selectively converting liquid photopolymers in a vat into solid pieces via a reflecting UV laser in a process called photopolymerization. SLA machines offer the highest accuracy but can only print one material at a time.

AM is still finding its place in medical imaging and new applications are being explored [2]. One of these is in the creation of phantoms for use with diagnostic imaging techniques.

Radiographic Scanning and Phantoms

The field of diagnostic radiology non-invasively generates images of patients to diagnose disease and guide treatment. The three major cross-sectional imaging modalities are ultrasound (US), computed tomography (CT), and magnetic resonance imaging (MRI). Imaging phantoms are synthetic models, usually of various portions of patient anatomy, which are designed to calibrate and optimize the equipment used by each modality. They are frequently used in quality assurance. Phantoms can also be used to train healthcare workers to perform image-guided procedures such as needle biopsy or intravenous cannula placement and allow trainees hands-on experience with realistic challenges. Researchers utilize phantoms to test new methods, ideas, and scenarios, such as radiation levels, in a safe way.

The Need for Customization

Commercially available phantoms can present significant limitations. While mass production models can be sufficient for the purpose of calibration, these models tend to be too generic for specialized scenarios, such as patient simulations. The common off-the-shelf models are usually adult-sized models with no opportunity for specification. Pediatric phantoms present a particular challenge due to the continuous change in patient size, relative proportions, and developmental anatomy. For example, many bones in children are at least partially cartilaginous (and are thus relatively weak and sensitive to injury) and slowly ossify throughout childhood. Children also present a wide variation in size, weight, and proportions depending on age that extend beyond the practical range of commercial phantoms. Furthermore, these models can be quite expensive, often retailing for thousands of dollars.

AM provides the opportunity to design customized phantoms for particular research interests [3] or even a specific patient's anatomy [4]. Because these phantoms can be as generic or specific as the training, surgical planning, or research requires, they allow researchers a wider range of flexibility than their ready-made counterparts. In clinical applications, these custom models can be used to practice, review, and train for complex and unusual cases. AM can offer significant cost savings compared to phantoms offered by medical companies, through reduction of the manufacturing process offered by the on-site production. The cost-benefit may be particularly evident for phantoms which are intended to be destroyed or damaged during their use (such as for interventional procedures). Furthermore, imaging phantoms can be made rapidly, increasing output and enabling the testing of ideas.

Knowledge of the expected imaging appearance of various materials as produced by each printer technology is necessary to guide imaging phantom development and to create new applications. Available literature describes the imaging appearance and characteristics of only a limited combination of targeted imaging modalities, printer technologies, and materials [3–18]. In addition, review articles aggregating these studies draw a conclusion without providing a direct-controlled comparison [19]. We sought to characterize the imaging appearance of a broad range of materials by three different printing processes and directly evaluate the outcomes on three cross-sectional diagnostic imaging modalities.

Materials and Methods

Three experiments were conducted: comparative scanning of a phantom incorporating all material

options from the three most common AM machines, evaluation of the blending material options offered by the PolyJet, and assessment of the impact of phantom shape in sonography using a spherical sample. A custom phantom was designed and fabricated in-house for each of these considerations.

The Printer Style phantom was constructed as a solid, rectangular silicone block containing the most common materials from each of the three selected styles of AM. Materials evaluated are acrylonitrile butadiene styrene (ABS) and acrylonitrile styrene acrylate (ASA) from FDM, VeroClear, and Tango from PolyJet, and VisoClear from SLA. Specific machines used are outlined in Table 1 in the Appendix with specifications and as representative machines for each category. This phantom comprised a number of small 45 × 26 × 6.5 mm sampling blanks that were printed and then embedded into a poured silicone block 75 mm high. The silicone pour for each of the phantoms was performed using a traditional two-part silicone rubber with a Shore durometer scale value of 10 A (Fig. 1 in the Appendix).

The blended PolyJet material phantom (Fig. 2 in the Appendix) focused on the unique multi-material part capabilities of this technology. Numerous 45 × 26 × 6.5 mm sampling blanks were created using each of the current PolyJet material options (polycarbonate, rubbers, and ABS). To test the potential of the blended material, a sample of each composite blend was printed on a connected gradient bar. The blended gradient bar (45 × 187.5 × 6.5 mm) was designed with a 12.5-mm step of each mixture of VeroWhite and Tango+ materials by Stratasys (Eden Prairie, USA).

A third phantom was fabricated with PolyJet materials printed in 20-mm diameter spheres that were embedded in a 75-mm high poured silicone block (Fig. 3 in the Appendix) specifically for the evaluation of ultrasound.

Imaging the Phantoms

Uniform Method

Ultrasound, CT, and MR technologists scanned the multi-material comparative, Printer Style phantom using their respective scanning modalities with a standardized protocol to ensure consistency. Each phantom was uniformly oriented to ensure the sample corresponded to the map. The acquired images were then evaluated for echogenicity, signal intensity, and radiodensity, respectively. Signal intensity, Hounsfield unit value, and dimensional measurements were evaluated using two common segmentation software platforms; TeraRecon (Foster City, USA) and Materialise Mimics (Leuven, Belgium). The dimensional accuracy of the printed phantoms was evaluated to assess the accuracy of phantom object dimensions. The specifics for each modality are outlined in the sections below.

Modality Testing

Under ultrasound, all three phantoms were imaged sample by sample using the abdomen settings with linear 6–15 MHz and curved 2–9 MHz probes. The cross-sections were captured in a single still image centered over each sample, and then labeled and exported using the model GE Logiq E9 (Boston, USA) with a frequency of 50–80 Hz.

The process for CT evaluation of the Printer Style phantom and PolyJet phantoms included each being scanned helically using a 128-slice Siemens Somatom Definition Flash 2012 (Munich, Germany) with CARE kV (adaptive peak kilovoltage and milliampere settings) and a 0.6 pitch. The image set was acquired at 0.6 mm and reconstructed in 2 mm.

For the MRI process, the Printer Style phantom and PolyJet phantoms were scanned using Siemens MAGNETOM Vida (Munich, Germany), a 3.0 Tesla strength scanner, using a 2-mm slice thickness with following sequences: Gradient/Inversion Reconstruction.

Image Analysis

Image analysis was performed separately in both Mimics and TeraRecon to control for potential differences in how the programs may analyze the images. For MRI and CT scans, measurements were obtained as either the mean signal intensity or Hounsfield unit value, respectively, of a 30 × 15 mm area in the center of each sample blank in both Mimics and TeraRecon. MRI images were viewed and qualitatively compared at the default grayscale levels for the modality and not further modified. CT images were viewed and qualitatively compared at traditional soft tissue window levels (window width 400 HU, window center 50 HU) and at a narrow window (80 HU, widow center 110). The length and width of the sample were measured in Mimics and compared to the original printing dimensions.

Results

Ultrasound

In all three phantoms, US scanning provided clean penetration through the silicone and clearly defined the upper and lower edges in each of the rectangular sample materials. US of the phantom containing spheres (Fig. 3 in the Appendix) showed a clear outline of the upper surface and a faint trace of the lower creating the shape. There was no discernible variation in internal echogenicity between the various samples in the comparative phantom. Specifically, there was no visible difference in echogenicity among the Tango material, Shore 27A, and hard plastics. Dimensional accuracy was not evaluated for ultrasound.

CT

The CT images of the Printer Style phantom (Fig. 1 in the Appendix) and PolyJet phantoms (Fig. 2 in the Appendix) showed a variation between the samples and the poured silicone of the surrounding block. Segmenting software revealed a noticeable variation in Hounsfield units between the material generated by SLA (378 HU), FDM (112 HU), and PolyJet (145 HU). In the PolyJet phantom, the plastic and rubber materials varied between 82 HU to 145 HU, respectively. The variation was not gradual in the printer-generated composite materials but rather a sharp change mid-bar was visualized, depicted best in the capture with very modified windowing. It was anticipated that a gradual change in the Hounsfield units would be seen correlating with the ratio of plastic and rubber across the sections of the bar. A high-dimensional accuracy was also confirmed in this scan within $1.55 \pm .6$ mm.

MRI

Scans of the Printer Style phantom (Fig. 1 in the Appendix) MRI revealed no distinctive variation in the signal intensities of the various materials. The only intensity variation was between the PolyJet material and its support material seen in the bottom right of the PolyJet phantom (Fig. 2 in the Appendix) and in the circles seen on the bottom center of the Printer Style phantom (Fig. 1 in the Appendix). The thresholds of the PolyJet phantom MRI scanning showed different signal intensities between the model (mean value of 17) and printer support (mean value of 778). A high-dimensional accuracy was also confirmed in this scan within $1 \pm .5$ mm.

Discussion

Material Development

One interesting note is the variation between the VisoClear and VeroClear. Each of these materials is described as polycarbonate—which should have a similar formulation by their respective manufacturing company; however, they showed a significant difference of 200 Hounsfield units when scanned. This variation in formulation could be used to create physically similar materials with varied scan properties. In turn, this illustrates that assumed similarities of traditional plastics do not inherently transfer to their AM counterparts. In the PolyJet phantom, the materials are visible but there is a little distinction between Tango and VeroWhite in their HU thresholds. However, in addition to the standard windowing described in the procedure, when the window width of the image is narrowed to a window width of 80 HU with a center at 110, the gradient is clearly visible. This is a promising observation, as this distinction could be emphasized through material and post-processing display research, presenting the opportunity for deliberate variation in models. No single printing style could produce materials with the range of densities required to represent complex patient anatomy such as an abdomen.

Material research and development for use in AM presents the possibility of new physical and imaging properties. Potential areas of research could include the development of softer, more compliant materials as well as varied properties of echogenicity, density, and proton relaxivity. Two such examples are the new Agilus30 and BioMimics materials released by Stratasys (Eden Prairie, USA). Each of these materials is softer (lower Shore durometer scale value) for increased flexibility. These materials are currently limited in access but there has been a promising discussion on potential widespread release. While these materials allow for improvement in the tactile qualities of phantoms, there has also been growing research in altering the imaging properties of existing materials. This includes mixing materials such as iodine [14], metal flecks [11], fiber, and sand. The combination of these materials in different ratios allow printing at various densities. These blended materials, however, can be temperamental and have the potential to damage the printer. They can also settle and alter curing processes; experimentation in this field tends to be limited to expendable machines.

Two-Phase Molding

While the ideal method to create a phantom would be a single print consisting of multiple parts, another way to achieve the same goal would be to use 3D prints as part of the fabrication process or to suspend within other materials. Viewing printing as a step in the fabrication process rather than solely as the end product allows for a larger selection of materials that may not currently be compatible with any AM process. Fluid-filled pockets can also be created by molding around a print that can be extracted and filled with another substance [6, 7]. These molds can also be repeatedly used as well as in succession for constructing parts or certain features [8, 13, 18]. This is the process of molding parts then transferring to a new mold with more detail to embed the first part, such as the bone, fat, and then skin.

AM holds great promise for the development of imaging phantoms. Many materials are visible with high-dimensional fidelity at cross-sectional imaging but provide limited ability to distinguish between various materials. Currently, these materials are best used for simple anatomic models such as bony structures or as molds that can be filled with materials demonstrating varied imaging appearances. A multi-modal approach is necessary to create an even moderately complex model.

Conclusion

The imaging properties of AM materials offer an opportunity to create highly dimensionally accurate, one- or two-material phantoms (Table 2 in the Appendix). However, these materials cannot currently be extended to complex multi-material applications to simulate the imaging properties of the human tissue through the process of direct printing.

Ultrasound

Current AM materials are limited to one printing material for use in US due to the indistinguishable echogenicity of each of the test materials across the machine platforms. The spherical phantoms confirmed that the sonographic properties were consistent across curved shapes as compared to flat regions allowing for complexity in cross-structure design. For these cases, the best potential for an ultrasound phantom would be various suspended parts that can be identified more by location or shape rather than their echogenicity. Such applications could include bone structures or to serve as containers for other sonographic materials for scanning such as a lung or gallbladder.

CT

The CT scans of both the multi-material comparative and PolyJet phantoms showed variation in the densities as measured by Hounsfield units. The most common material from each of the three AM styles (VisoClear, ABS, ASA, VeroClear, and Tango) demonstrated significant differences in densities that could be used to represent different tissues in a variety of anatomic models (Table 3 in the Appendix).

Imaging phantoms present the best opportunity to create complex printed models for CT. Although currently, this would require modified windowing or use of multiple printers, this is clearly a potential opportunity in the development of the material formulations for phantom creation.

MRI

For the multi-material and PolyJet phantoms (Figs. 1 and 2 in the Appendix), the variation between the model materials is impossible to distinguish with one notable exception: the support material used in the creation of the parts offered a significantly different grayscale visualization. This means that the support material could be used to simulate additional regions with the model materials. However, it is important to remember that this material is designed to dissolve or be washed away and its use would require careful handling or containment within a specialized shell. Similar to ultrasound, the MRI applications are currently limited to one or two distinct model sections or regions or for the purpose of housing other MRI distinctive materials.

Acknowledgments We would like to thank Glenn Ferrick (MR), Patricia Mecca (CT/MR), Colleen Flowers (CT), Lamont Hill (US), Marcy L. Hutchinson (US), and team for assisting in the scan of phantoms.

Availability of Data and Materials Data will be made available on request. The authors have the right to share the data used in this research and will provide it upon request.

Authors' Contributions ES and RS participated in the conception and design of the study, data analysis, and interpretation. ES fabricated models and oversaw scanning. KB and ES completed scan interpretation and data collection. All authors drafted the manuscript and approved the final version.

Compliance with Ethical Standards

Competing Interest The authors declare that they have no conflict of interest.

Appendix

Table 1 Machine details. Details of each printing style used in this study

	Machine details			
	Machine	Company	Resolution	Materials
SLA	Projet 6000HD	3D Systems Rock Hill, USA	0.004 in. (0.1 mm)	VisoClear
FDM	Fortus 450mc	Stratasys, Ltd Eden Prairie, USA	0.005 in. (0.13 mm)	ABS ASA
PolyJet	Connex 500	Objet/Stratasys, Ltd Eden Prairie, USA	28 μm (0.0011 in.)	Tango+ VeroWhite Support

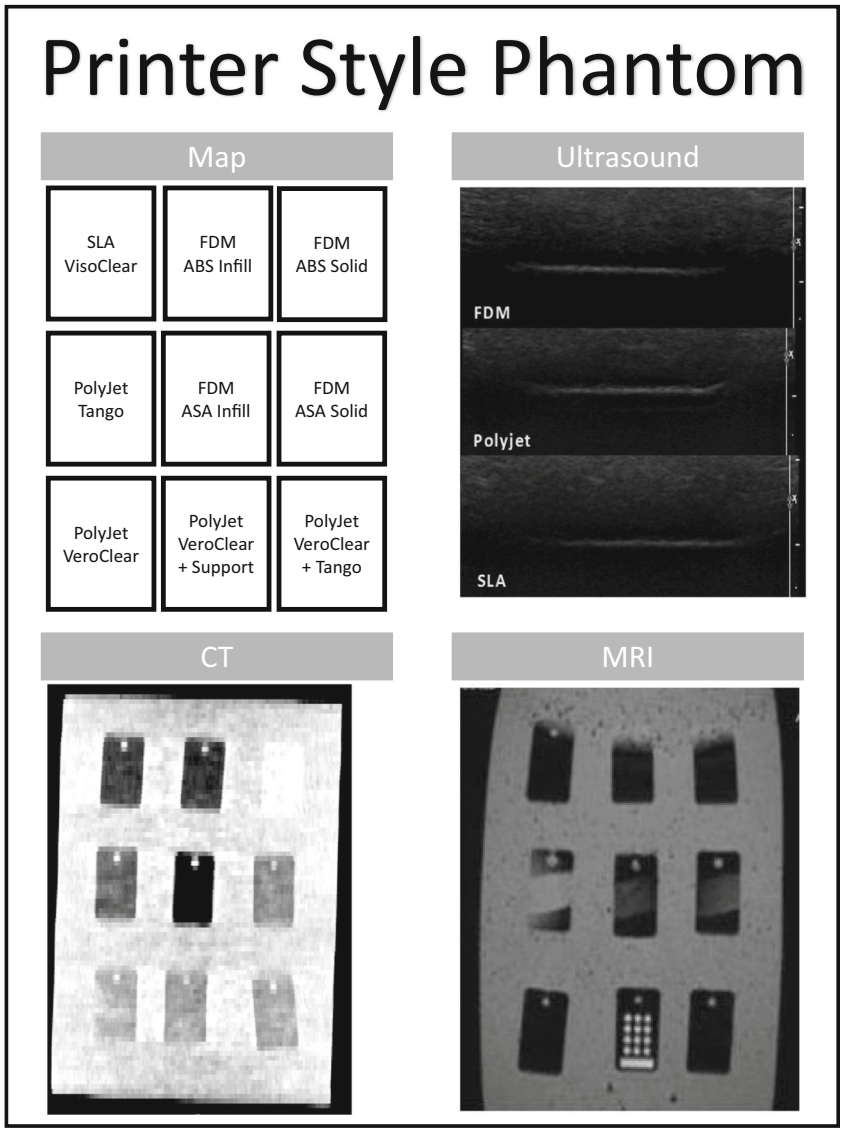

Fig. 1 Printer Style phantom. Contains the sample part map and images of the phantom under ultrasound, CT, and MRI for the Printer Style phantom

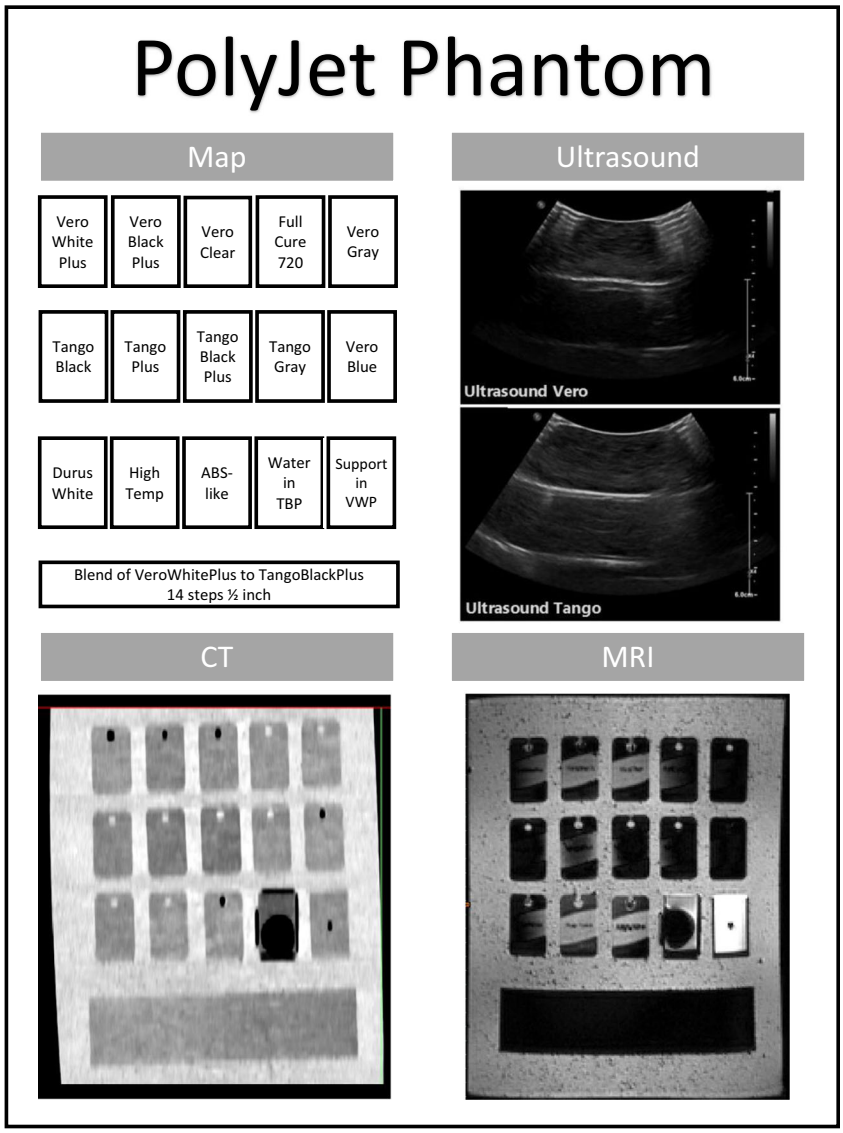

Fig. 2 PolyJet Phantom. Contains the sample part map and images of the phantom under ultrasound, CT, and MRI for the PolyJet phantom

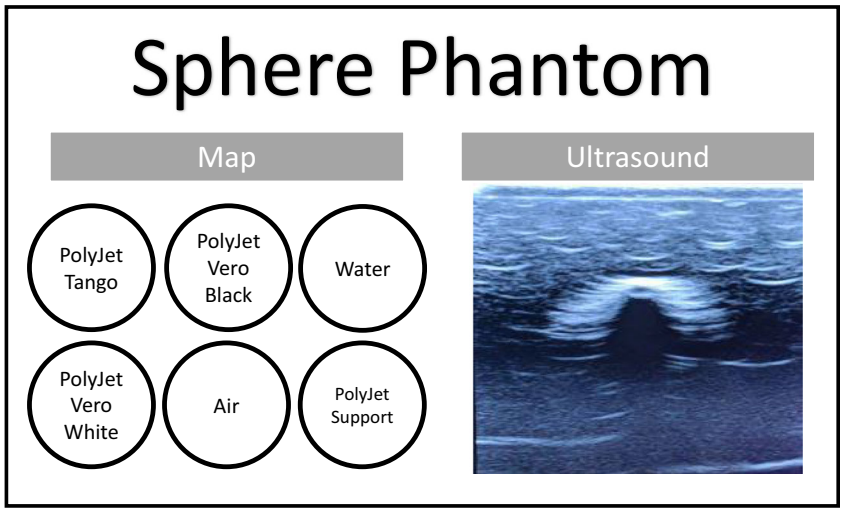

Fig. 3 Sphere Phantom. Contains the sample part map and the image under ultrasound for the Sphere phantom

Table 2 Method-application chart. This chart summarizes the potential application of each printing style and its application in the production of phantoms

	Method-application chart		
	Ultrasound	CT	MRI
SLA	✓ Simple 1–2 material phantoms	✓ Simple 1–2 material phantoms	✓ Simple 1–2 material phantoms
FDM	✓ Simple 1–2 material phantoms	✓ Simple 1–2 material phantoms	✓ Simple 1–2 material phantoms
PolyJet	✓ Simple 1–2 material phantoms	✓ Simple 1–2 material phantoms ✓ Moderate complexity with modified windowing	✓ Simple 1–2 material phantoms
Mixed Machine Methods	No additional advantage	✓ Simple 1–2 material phantoms ✓ Moderate complexity	✓ Simple 1–2 material phantoms ✓ Moderate complexity

Table 3 Hounsfield comparison chart. This chart compares each of the printed materials to anatomical features with comparable Hounsfield values

Hounsfield Comparison Chart		
	HU	Hounsfield comparison
SLA VisoClear	371.23	Contrast or craniofacial bone
FDM ABS Infill	− 86.71	Fat
FDM ABS Solid	57.52	Liver or clotted blood
FDM ASA Solid	16.57	Cerebrospinal fluid, bile, urine
FDM ASA Infill	− 743.2	Between lung and air
PolyJet VeroClear	146.57	Soft tissue, contrast, or mucus
PolyJet Tango	98.09	Gallstones

References

1. George E, Liacouras P, Rybicki FJ, Mitsouras D: Measuring and establishing the accuracy and reproducibility of 3D printed medical models. RadioGraphics. 37(5):1424–1450, 2017. https://doi.org/10.1148/rg.2017160165
2. Mitsouras D, Liacouras P, Imanzadeh A, Giannopoulos AA, Cai T, Kumamaru KK, George E, Wake N, Caterson EJ, Pomahac B, Ho VB, Grant GT, Rybicki FJ: Medical 3D printing for the radiologist. RadioGraphics. 35(7):1965–1988, 2015. https://doi.org/10.1148/rg.2015140320
3. Eley KA, Watt-Smith SR, Golding SJ: "Black bone" MRI: A novel imaging technique for 3D printing. Dentomaxillofacial Radiol Dentomaxillofac Radiol. 46:46, 2017. https://doi.org/10.1259/dmfr.20160407
4. Leng S, Chen B, Vrieze T, Kuhlmann J, Yu L, Alexander A, Matsumoto J, Morris J, McCollough CH: Construction of realistic phantoms from patient images and a commercial three-dimensional printer. J Med Imaging. 3:033501, 2016. https://doi.org/10.1117/1.JMI.3.3.033501
5. Matsumoto JS, Morris JM, Foley TA, Williamson EE, Leng S, McGee KP, Kuhlmann JL, Nesberg LE, Vrtiska TJ: Three-dimensional physical modeling: Applications and experience at Mayo Clinic. RadioGraphics. 35(7):1989–2006, 2015. https://doi.org/10.1148/rg.2015140260
6. Wood S, Krishnamurthy N, Santini T, Raval S, Farhat N, Holmes JA, Ibrahim TS: Design and fabrication of a realistic anthropomorphic heterogeneous head phantom for MR purposes. PLoS One. 12, 2017. https://doi.org/10.1371/journal.pone.0183168
7. Kasten JA, Vetterli T, Lazeyras F, Van De Ville D: 3D-printed shepp-Logan phantom as a real-world benchmark for MRI. Magn Reson Med. 75:287–294, 2016. https://doi.org/10.1002/mrm.25593
8. Hazelaar C, Van Eijnatten M, Dahele M, et al: Using 3D printing techniques to create an anthropomorphic thorax phantom for medical imaging purposes. 2017.
9. Cerviño L, Soultan D, Cornell M, Yock A, Pettersson N, Song WY, Aguilera J, Advani S, Murphy J, Hoh C, James C, Paravati A, Coope R, Gill B, Moiseenko V: A novel 3D-printed phantom insert for 4D PET/CT imaging and simultaneous integrated boost radiotherapy. Med Phys. 44:5467–5474, 2017. https://doi.org/10.1002/mp.12495
10. Javan R, Cho AL: An Assembled Prototype Multimaterial Three-Dimensional–Printed Model of the Neck for Computed Tomography– and Ultrasound-Guided Interventional Procedures. https://doi.org/10.1097/RCT.0000000000000630
11. Ceh J, Youd T, Mastrovich Z, Peterson C, Khan S, Sasser T, Sander I, Doney J, Turner C, Leevy W: Bismuth infusion of ABS enables additive manufacturing of complex radiological phantoms and shielding equipment. Sensors (Switzerland). 17, 2017. https://doi.org/10.3390/s17030459
12. Shin J, Sandhu RS, Shih G: Imaging properties of 3D printed materials: multi-energy CT of filament polymers. J Digit Imaging. 30:572–575, 2017. https://doi.org/10.1007/s10278-017-9954-9
13. Adams F, Qiu T, Mark A, Fritz B, Kramer L, Schlager D, Wetterauer U, Miernik A, Fischer P: Soft 3D-printed phantom of the human kidney with collecting system. Ann Biomed Eng. 45:963–972, 2017. https://doi.org/10.1007/s10439-016-1757-5
14. Jahnke P, Limberg FRP, Gerbl A, Ardila Pardo GL, Braun VPB, Hamm B, Scheel M: Radiopaque three-dimensional printing: A method to create realistic CT phantoms. Radiology. 282:569–575, 2017. https://doi.org/10.1148/radiol.2016152710
15. Mitsouras D, Lee TC, Liacouras P, Ionita CN, Pietilla T, Maier SE, Mulkern RV: Three-dimensional printing of MRI-visible phantoms and MR image-guided therapy simulation. Magn Reson Med. 77:613–622, 2017. https://doi.org/10.1002/mrm.26136
16. West SJ, Mari JM, Khan A, Wan JHY, Zhu W, Koutsakos IG, Rowe M, Kamming D, Desjardins AE: Development of an ultrasound phantom for spinal injections with 3-dimensional printing. Regional Anesthesia and Pain Medicine. 39:429–433, 2014. https://doi.org/10.1097/AAP.0000000000000136

17. Bieniosek MF, Lee BJ, Levin CS: Technical note: Characterization of custom 3D printed multimodality imaging phantoms. Med Phys. 42:5913–5918, 2015. https://doi.org/10.1118/1.4930803
18. Gatto M, Memoli G, Shaw A, Sadhoo N, Gelat P, Harris RA: Three-dimensional printing (3DP) of neonatal head phantom for ultrasound: Thermocouple embedding and simulation of bone. Med Eng Phys. 34:929–937, 2012. https://doi.org/10.1016/j.medengphy.2011.10.012
19. Filippou V, Tsoumpas C: Recent advances on the development of phantoms using 3D printing for imaging with CT, MRI, PET, SPECT, and ultrasound. Med Phys. 45:e740–e760, 2018. https://doi.org/10.1002/mp.13058